

Transient liquid phase bonding of Sn–Bi solder with added Cu particles

Omid Mokhtari¹ · Hiroshi Nishikawa¹

Received: 9 November 2015 / Accepted: 3 January 2016 / Published online: 9 January 2016
© Springer Science+Business Media New York 2016

Abstract The aim of this study was to apply the transient liquid phase (TLP) bonding technique to low-temperature Sn–Bi-based solders to enable their use in high-temperature applications. The microstructure of the eutectic Sn–Bi solders with and without added Cu particles was investigated with the solders sandwiched between two Cu substrates. The flux of the Cu atoms successfully consumed the Sn phase and resulted in the formation of Sn–Cu intermetallic compounds and a Bi-rich phase in the solder joint. This caused the melting point of the solder joint to increase from 139 to 201 °C. The results of this study show the potential of using low-temperature solders in high-temperature applications. This study also provides new insight into the advantages of using particles in the TLP bonding process.

1 Introduction

Solder joints are one of the main materials for interconnects in microelectronic packaging; they must form reliable electrical and mechanical connections that retain their integrity throughout the subsequent manufacturing process and operating conditions. Sn–Pb solder alloys have been widely used in the electronics industry to connect electronic devices to substrates because of their excellent properties. However, because of the harmful effects of Pb on human health and the environment, the use of Pb in the electronics industry has been restricted. Therefore, Pb-free

solders have replaced the conventional Sn–Pb solders. Sn–Bi solder has been recognized as a promising substitute because its mechanical properties are comparable to that of Sn–37Pb (the number represents the mass%) eutectic solder alloy [1–3]. The eutectic composition of the Sn–Bi system is Sn–58Bi, which has a melting point of 139 °C.

Low-temperature soldering is necessary when the devices to be soldered are prone to thermal damage. Some of the major failure mechanisms of integrated circuit packages, such as warpage, whisker growth, delamination, and internal cracking, are caused by the high temperatures during the solder reflow process [4–8].

Even though the low melting point of Sn–Bi solder is an advantage for low-temperature soldering, it means Sn–Bi solder can only be used for applications with working temperatures below 139 °C [9]. One method that can increase the melting point of solder during processing is transient liquid phase (TLP) bonding. TLP bonding consists of the isothermal solidification of an initially molten joint through the disappearance of the liquid as a result from the interaction between the molten solder and the substrates and formation of solid IMC phases(s) [10–12]. Thus, a TLP joint can be processed at a relatively low temperature, but results in the formation of a new in situ alloy with a higher re-melting point. Recently, the application of TLP processing to low-temperature soldering in the microelectronics industry has attracted more interest. The principle behind TLP processing is the solid–liquid interdiffusion (SLID) between the atoms of two materials, and has been primarily applied to the low-temperature bonding of power semiconductor dies [13].

Several studies have reported the application of TLP techniques, e.g., the fluxless soldering of multilayers of Sn–50Cu [14, 15], Ag–20In [16], and Au–20Sn [17], for die attachment processing [18]. However, there has been little

✉ Omid Mokhtari
mokhtari@jwri.osaka-u.ac.jp

¹ Joining and Welding Research Institute, Osaka University,
11-1 Mihogaoka, Ibaraki, Osaka 567-0047, Japan

research on applying this technique to the solder pastes used in conventional soldering applications, which could be used to replace common Pb-free solders (e.g., Sn–Ag–Cu, melting point = 217 °C). In addition, in these studies, the low-melting-point phase is consumed by the base metals on either side of the joint through dissolution, which forms a bulk interlayer. However, in the case of large joints, the consumption of the low-melting-point phase, especially deep in the middle of a joint, takes a considerable amount of time because of the relatively large distances separating the solid solute from the base metals on either side [19, 20].

The TLP technique can also be used to create Sn–Bi-based solders that are suitable for high-temperature applications. This involves converting the entire Sn phase of the solder to Sn–Cu intermetallic compounds (IMCs) by adding a sufficient concentration of Cu particles to the solder before being reflowed. The behavior of a ternary alloy system during TLP processing has been previously investigated [21], and the compositional shifts during the TLP processing of a ternary Sn–Bi–Cu system have recently been reported by others [22]. However, the microstructural transformation in this system and analysis of the remaining eutectic phase require further study. Figure 1 shows a schematic of the conversion of eutectic Sn–Bi solder into Sn–Cu IMCs and a Bi-rich phase.

The addition of Cu particles to the solder allows the Sn phase to be consumed not only by the flux of Cu atoms from the substrate, but also by the Cu particles that are distributed throughout the joint. The added metallic particles and molten solder react during reflow, which results in the nucleation and growth of IMC, at the particle/solder interface [23–25], consuming the entire Sn phase and leaving only Sn–Cu IMCs and a Bi-rich phase in the solder joint that causes isothermal solidification. The IMC formation due to the reflow process is directly related to the

temperature–time profile of the reflow process while the solder is in a liquid state [26]. The addition of Cu particles has another advantage; if considering a constant volume, the larger surface area:volume ratio of Cu particles compared to that of a Cu substrate provides a larger contact area, which in turn allows more reactions to occur between Sn and Cu atoms.

However, one of the major concerns when adding reactive particles to the solder paste is preventing them from being expelled from the joints along with the flux during the reflow process. Therefore, the probability that the particles are trapped within the solder joint depends on the probability of encountering a solder surface or being captured at the surface before leaving the solder paste. Thus, the surface of particles without a protective coating can be oxidized, which increases the probability of being expelled from the solder. The probability of being captured is further decreased by using nano-scale particles [27]. Therefore, because the primary experiments in this study using particles in a nano size range resulted in the expelling of particles due to the oxidation, the Cu particles used in this study are with the diameters of 5 μm .

The aim of this study was to investigate the TLP bonding process of a Sn–Bi solder with added Cu particles to increase the melting point of the solder joint. In addition, the interfacial microstructure between the solder and Cu substrate and particles were studied.

2 The TLP bonding process

According to the comprehensive description given in the review article by Zhou et al. [28], the TLP bonding process can be divided into four major stages. Stage 1 is the heating stage where the component is heated from room temperature to the melting point of the filler metal, which is

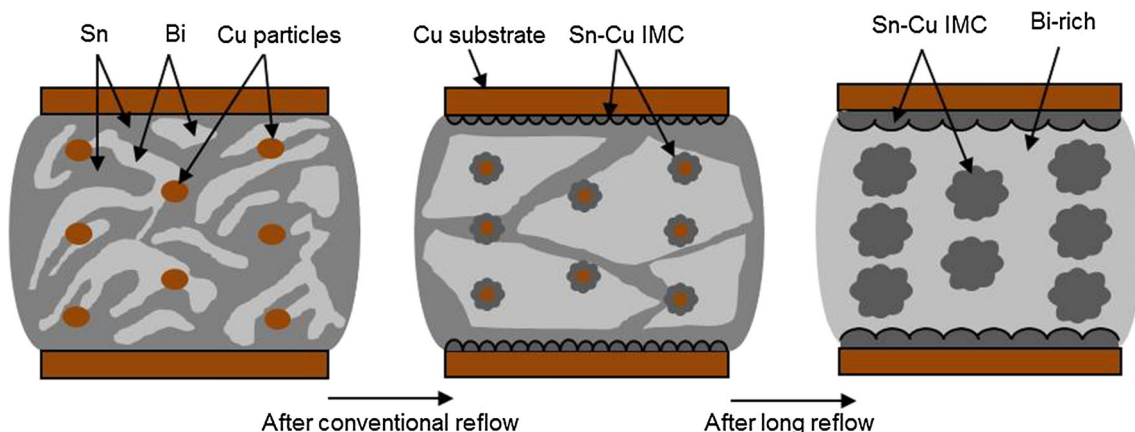


Fig. 1 The schematic illustration of the conversion of the eutectic Sn–Bi to the Sn–Cu IMCs and Bi

eutectic solder in the case of this study. Once the eutectic temperature is reached, the eutectic solder melts, wetting the Cu particles and substrates. As the temperature continues to increase, the compositions of the solid Cu (C_S ; both particles and substrates) and liquid solder (C_L) at the solid/liquid interface follow the phase boundaries that are predicted by the phase diagram. This is followed by stage 2, the dissolution stage, where the Cu particles dissolve into the liquid phase and the size of the liquid phase increases. The liquid phase increases in size to maintain the mass balance, as is explained below in Eq. (1) [29]:

$$(C_L - C_S) \cdot \frac{d}{dt} X(t) = D_S \cdot \frac{\partial}{\partial x} C_S - D_L \cdot \frac{\partial}{\partial x} C_L \quad (1)$$

where $X(t)$ is the position of the solid/liquid interface, and D_S and D_L are the solute diffusivities in the solid and liquid phases, respectively. Stage 3 is the isothermal solidification stage where the liquid phase solidifies. During this stage, the concentration of the liquid phase predominated by Sn decreases continuously. Finally, stage 4 is the homogenization of the solder joint and can occur wherever solid-state diffusion takes place. In this study, stages 1, 2, and 3 were applied to investigate the eutectic Sn–Bi phase as functions of the applied time and temperature.

3 Experimental procedure

3.1 Alloy and solder preparation

In this research, two solder alloys were used: Sn–Bi and Sn–Bi with added Cu particles (30 mass%). The solder pastes were prepared by Senju Metal Industry Co., Ltd. which were made of eutectic Sn–Bi, Cu particles ($\varnothing 5 \mu\text{m}$, Mitsui Mining and Smelting Co., Ltd., code: 1400Y) and 11 mass% flux. Figure 2a shows a scanning electron microscopy (SEM) image of the Cu particles. The diameter of approximately 100 Cu particles was measured with

quantitative analysis software, and the resulting particle-size distribution is shown in Fig. 2b. The paste was deposited onto the top of a Cu plate ($\varnothing 10 \text{ mm} \times 5 \text{ mm}$) after it was cleaned with HCl and ethanol in an ultrasonic bath by printing through a 150- μm -thick stencil. The bondline thickness of the solder paste before reflow was 150 μm . Another Cu plate ($\varnothing 3 \text{ mm} \times 2 \text{ mm}$), which was cleaned by the same method, was placed on top of the paste to make a Cu/solder/Cu sandwich without applied pressure. Figure 3 shows a schematic of the solder joint samples.

3.2 Reflow process and cross-section preparation

The samples with added Cu particles were pre-heated at 100 °C for 150 s and then reflowed at 170, 200, or 230 °C for 1, 10, or 50 min. In addition, samples without Cu particles were also pre-heated at 100 °C for 150 s and then reflowed at 170 and 230 °C for 1 min and 6 h, respectively, for comparison. The samples were reflowed in a reflow oven (Sanyo Seiko SMT Scope SK-8000) under an N_2 atmosphere. Cross-sections of the joints were prepared with mechanical polishing. It was followed by chemically etching using colloidal silica suspension.

3.3 Microstructure of the solder joints

The microstructure of the solder joints was investigated with SEM (Keyence VE-8800), field emission SEM (FESEM, JEOL JSM-6500F), and a field emission electron probe microanalyzer (EPMA, JEOL JXA-8530F).

3.4 Differential scanning calorimetry (DSC) analysis

The DSC was performed with an Exstar 7020 to examine the enthalpy of the joints. The heating rate and isothermal period used were 10 °C/min and 10 min, respectively. In this study in addition to the Sn–Bi–30Cu solder paste and

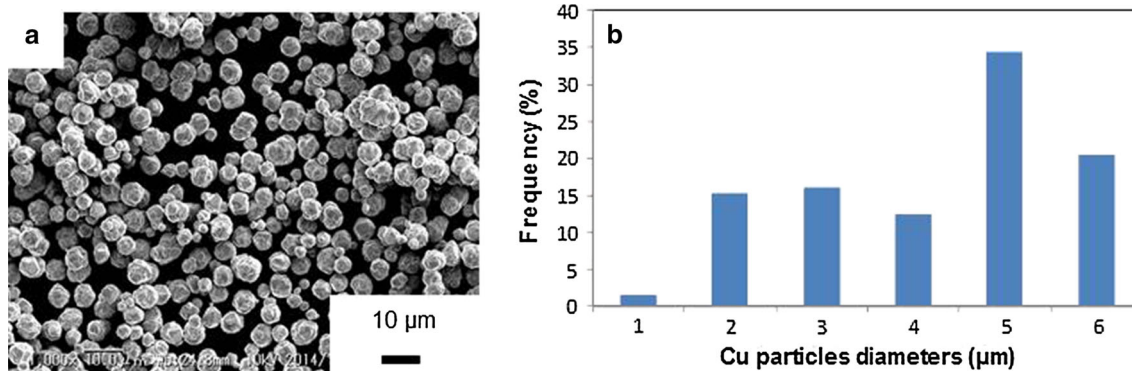


Fig. 2 a SEM image of Cu particles before addition to the solder paste and b the frequency of Cu particles diameters

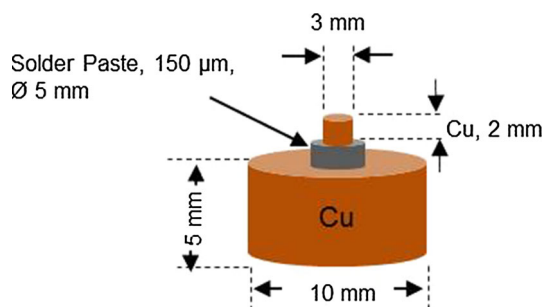


Fig. 3 The schematic illustration of the solder joint sample

solder bulk, Cu/Sn–Bi–30Cu/Cu solder joints were also examined by DSC after removal from the Cu substrates. The mass of the samples used for the DSC measurements ranged from 5.5 to 8.5 mg. The melting range of each valley was considered the difference between the solidus (hereinafter referred to as the melting onset) and liquidus points, which were calculated from the DSC measurements.

3.5 Elemental analysis

X-ray diffraction (XRD) measurements were performed with a diffractometer (Rigaku Ultima IV) using Cu–K α radiation ($\lambda = 1.5405 \text{ \AA}$) at an accelerating voltage of 40 kV. The diffracted beam was scanned in steps by 0.01° across a 2θ range of $10\text{--}100^\circ$. In addition, elemental mapping was performed with the EPMA.

4 Results

4.1 Estimating the Cu content required for TLP bonding

The scale of the reaction between the Sn and Cu to form Cu_6Sn_5 was investigated. This mathematical analysis only considered the reaction between the Sn atoms and added Cu particles; the flux of Cu atoms from the substrates was neglected (due to the significantly higher surface area of particles over substrate which the detail will be discussed later in this paper). To determine the concentration of Cu required to convert the entire Sn phase into IMCs, three Cu particle contents were theoretically investigated: 20, 30, and 40 mass%. By considering the atomic weights of Cu, Sn, and Bi which are 63.547, 118.710, and 208.980, respectively, the atomic percentages of Cu, Sn, and Bi required for the Sn–Bi + 20 mass% of Cu solder were 38.5, 34.5, and 27.0 %, respectively. By similar calculations, the atomic percentages of Cu, Sn, and Bi were 51.4, 27.3, and 21.3 % for the Sn–Bi + 30 mass% of Cu solder

and 62.5, 21.0, and 16.5 % for the Sn–Bi + 40 mass% of Cu solder, respectively. These values are summarized in Table 1, where they are used to calculate the percentage of unreacted Sn–Bi or unreacted Cu expected in the system assuming formation of Cu_6Sn_5 IMCs only.

Even though Cu_3Sn is a more stable phase than Cu_6Sn_5 , the latter forms earlier and Cu_3Sn is a product of the reaction of Cu_6Sn_5 and Cu substrate [12]. Thus, the formation of Cu_3Sn would not affect the consumption of Sn from the eutectic Sn–Bi phase. Therefore, for this analysis, it was assumed that all Sn and Cu particles fully react to form the Cu_6Sn_5 IMC. Thus, in the case of the Sn–Bi alloy with 20 mass% of Cu, all of the Cu particles would react with the Sn to form Cu_6Sn_5 and leave 4.29 % of the eutectic Sn–Bi phase and 25.12 % of the Bi-rich phase in the solder. For the Sn–Bi + 30 mass% of Cu alloy, all of the Sn phase would react with the Cu to form Cu_6Sn_5 and leave 18.64 % of the Cu phase in the solder. Finally, for the Sn–Bi + 40 mass% of Cu alloy, all of the Sn phase would react with the Cu and leave 37.3 % of unreacted Cu in the solder. Thus, only the Sn–Bi solders with 30 or 40 mass% of Cu have a sufficient concentration of Cu to react with and consume the entire Sn phase inside the solder. Therefore, the Sn–Bi solder with 30 mass% of Cu particles (hereinafter referred to as Sn–Bi–30Cu solder) was used in this study.

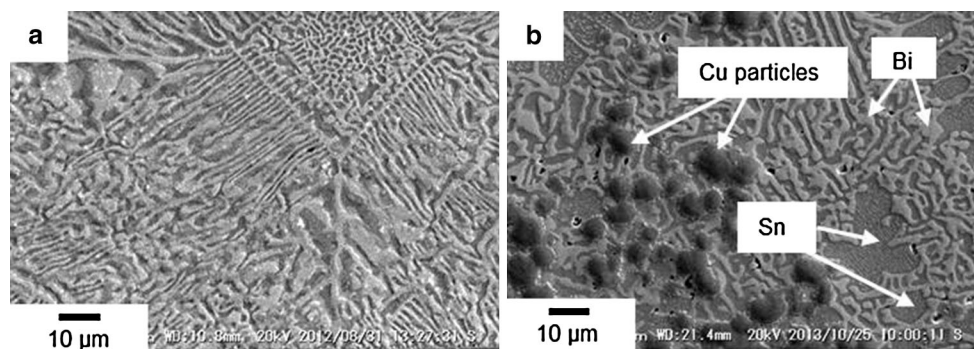
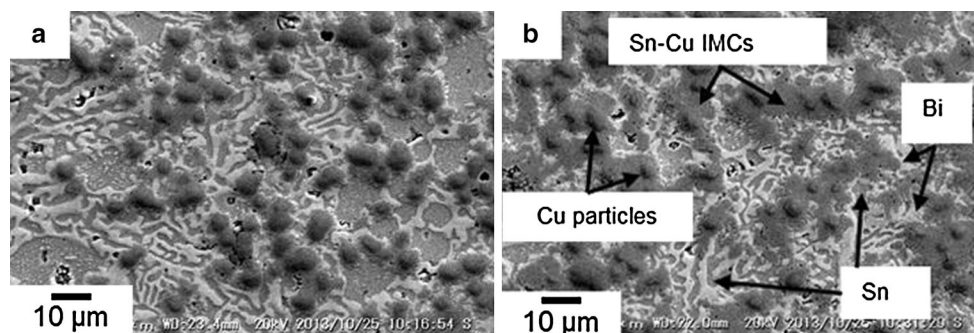
4.2 Microstructure of the solder joints

Figure 4 shows a comparison of the microstructure of the conventional Sn–Bi and Sn–Bi–30Cu solders after being reflowed at 170°C for 1 min. The bright and dark gray regions in the images represent the Bi and Sn phases, respectively. The dark spots in Fig. 4b are Cu particles that have partly reacted with the Sn phase. In addition, there is a very thin, sunflower-shaped IMC layer around each Cu particle. Even though the addition of Cu particles in this study is because of their advantage in reducing the reflow period in comparison with the Cu/Sn–Bi/Cu solder joint, to investigate the required reflow period for the complete isothermal solidification, investigation on the longer period of reflow is needed. Therefore, samples were subjected to 10 and 50 min reflow periods at 170°C . Figure 5 shows the different microstructures of the Sn–Bi–30Cu solder after being reflowed at 170°C for 10 and 50 min.

As can be seen, there is not a large difference between the thickness of the IMC layers around the Cu particles in Figs. 4b and 5a. However, Fig. 5b shows a large difference compared to the previous images, revealing that 50 min of reflow is highly effective for reacting Sn with Cu. On the other hand, even though Fig. 5b shows that the reactions between Sn and Cu increase significantly, the Sn and Bi phases are still clearly visible.

Table 1 Mathematical calculation of sufficient amount of Cu particle additions to convert the whole Sn phase to the Sn–Cu IMCs

	Mass% Cu	at.% Cu	at.% Sn	at.% Bi	Remained Cu at.%	Remained eutectic Sn–Bi at.%	Remained Bi-rich at.%
Sn–58Bi+	20	38.5	34.5	27	–	4.29	25.12
	30	51.4	27.3	21.3	18.64	–	21.3
	40	62.5	21	16.5	37.3	–	16.5

**Fig. 4** The microstructure of **a** Sn–Bi and **b** Sn–Bi–30Cu after reflow at 170 °C for 1 min**Fig. 5** The microstructure of Sn–Bi–30Cu after reflow at 170 °C for **a** 10 min and **b** 50 min

Therefore, reflow at 170 °C for 1, 10, or 50 min does not provide enough heat input for the complete reaction of the Sn phase with the added Cu particles, and thus, new reflow profiles at higher temperatures were tested. Figure 6 shows the microstructure of the Sn–Bi–30Cu solder after being reflowed at 200 and 230 °C for 1, 10, or 50 min. For both of these reflow temperatures, as the reflow period increases, the thickness of the layer of IMCs around the Cu particles also increases. This indicates that more reactions occur between the Sn phase and Cu particles as the reflow period increases. Of all the reflow periods and temperatures tested, only the samples reflowed at 200 and 230 °C for 50 min appear to have successfully completed the reaction between the Sn phase and Cu particles.

Figure 7 shows the EPMA elemental mapping results of the Sn–Bi–30Cu solder after being reflowed at 200 °C for

50 min. As can be seen, there are two Sn–Cu IMCs: one is a thin layer around the Cu particles and the other is the large phase distributed throughout the solder joint. According to the literature [30], it is well established that the two IMCs are the ϵ -phase (Cu_3Sn) compound that has grown around the Cu particles and η -phase (Cu_6Sn_5) compound adjacent to the solder.

To evaluate the effect of added Cu particles in reducing the required heat input for complete isothermal solidification, in addition to the Sn–Bi solder paste with added Cu particles, eutectic Sn–Bi paste without added Cu particles was subjected to reflow at 230 °C for 6 h and the cross-sectional microstructure is shown in Fig. 8. The reflow profile with significantly large heat input was attempted to achieve the complete isothermal solidification. However, as can be seen in Fig. 8, even

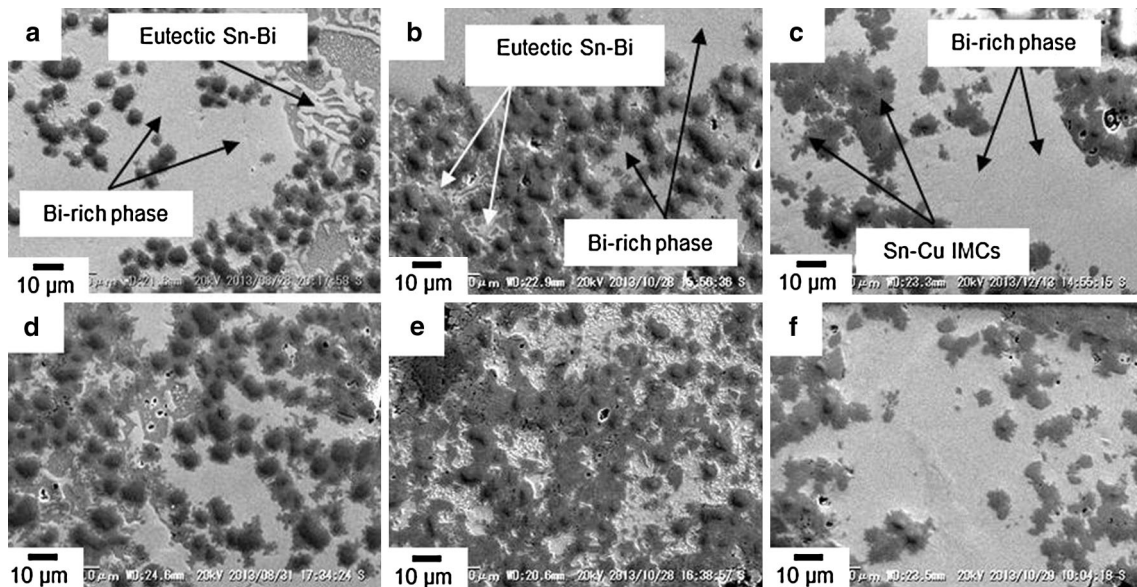


Fig. 6 The microstructure of Sn–Bi–30Cu after reflow **a** at 200 °C for 1 min, **b** at 200 °C for 10 min, **c** at 200 °C for 50 min, **d** at 230 °C for 1 min, **e** at 230 °C for 10 min, **f** at 230 °C for 50 min

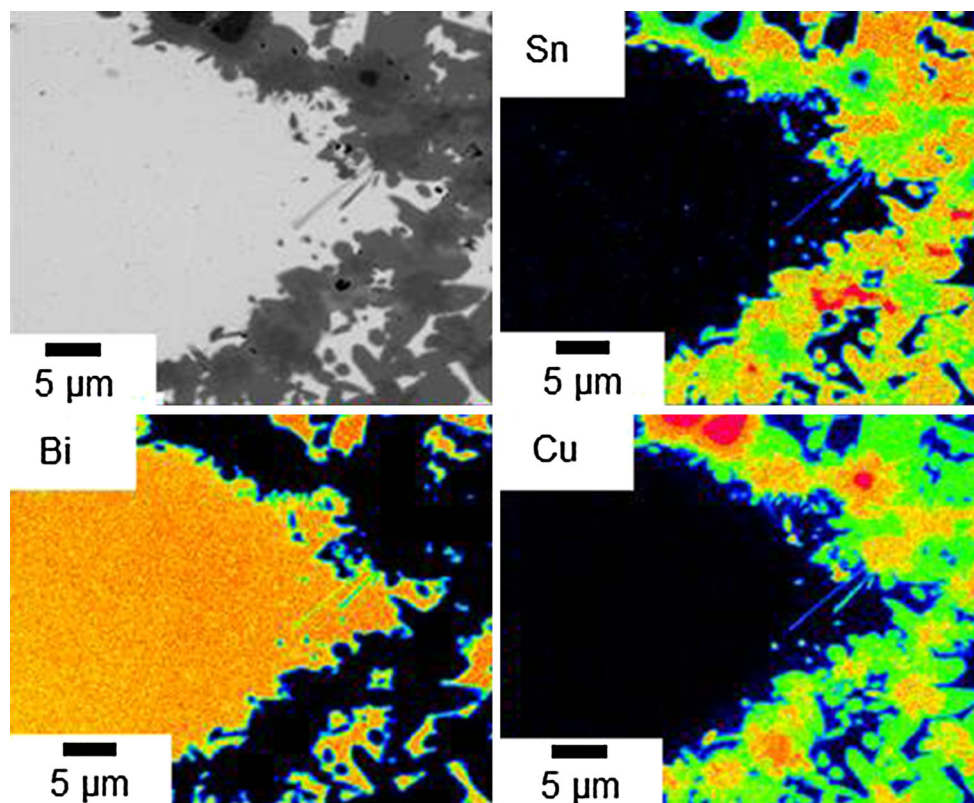


Fig. 7 The EPMA mapping results of the Sn–Bi–30Cu after reflow at 200 °C for 50 min

though a large IMC layer is formed within the solder joint, the eutectic Sn–Bi regions are still remained indicating the significant effect of added Cu particles in reducing the required heat input for isothermal solidification.

4.3 Spalling of the Cu_6Sn_5 IMC

One phenomenon of the solder/substrate reaction is the spalling of intermetallic compounds from the solder/substrate interface into the bulk solder. Figure 9 shows that after being reflowed at

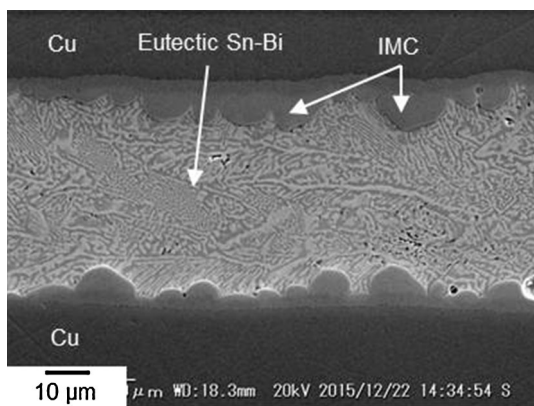


Fig. 8 The microstructure of eutectic Sn–Bi solder after reflow at 230 °C for 6 h

170 °C for 10 min, the Cu_6Sn_5 IMC spalls away from the Cu particles. However, the Cu_6Sn_5 IMC layer does not exhibit the same behavior at the Cu substrate. Figure 10 also shows that after being reflowed at 200 °C for 50 min, the Cu_6Sn_5 IMC layers on both the Cu particles and substrate show spalling behavior. As can be seen in Fig. 9c, d, the comet-like appearance of the Cu_6Sn_5 IMC shows the spalling direction.

4.4 Thermal analysis of the compositional shift by DSC

Figure 10 shows the DSC curves of the Sn–Bi–30Cu solder before and after the reflow treatment of both the bulk solder

and the solder sandwiched between Cu substrates. The microstructures of the solders tested are shown in Figs. 6b, c and 8e, f. In Fig. 10a, a melting event of the bulk solder occurs at approximately 139 °C, which represents the melting of the eutectic Sn–Bi phase. In addition, two valleys are present at approximately 667 and 700 °C, which represent the melting of the Cu_6Sn_5 and Cu_3Sn IMCs, respectively. Even though the solder paste does not contain these Sn–Cu IMCs, once the temperature reaches a certain level during the DSC test, it allows Sn and Cu to react and form the Sn–Cu IMCs. The DSC curves in Fig. 10b, c have a new valley indicating a melting event at approximately 201 °C.

Figure 10b shows that after the solder is reflowed at 200 °C for 10 min, peaks representing eutectic Sn–Bi and new melting event co-exist, while Fig. 10c shows that almost all the Sn phase has been consumed. In Fig. 10c, the curve representing the bulk solder with added Cu particles has a small valley at 139 °C, which represents the trivial amount of the eutectic Sn–Bi phase that has not reacted with the Cu particles. However, when the Sn–Bi–30Cu solder is sandwiched between Cu substrates and subjected to the same reflow profile (the dotted line), there is not a valley at 139 °C. The melting point of Bi is 271 °C, and therefore, the new valley in Fig. 10b, c does not represent the melting of Bi. The DSC results are summarized in Tables 2 and 3.

In Fig. 10a, the initial melting endotherm, $\Delta h_{\text{Eutectic}}$, is proportional to the area of the endothermic melting valley.

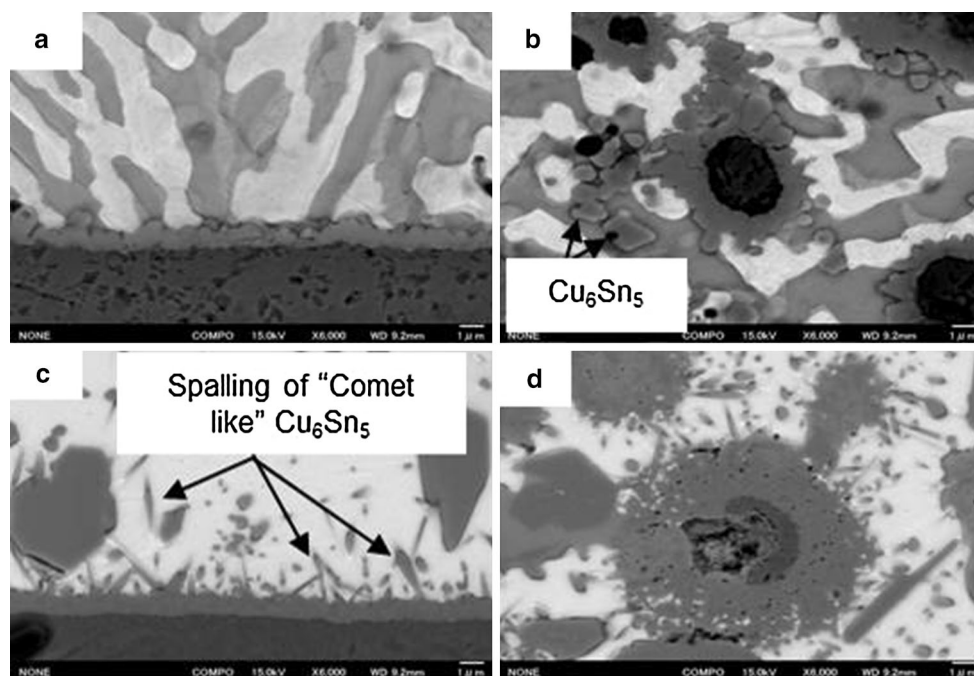


Fig. 9 The spalling of Cu_6Sn_5 interfacial IMCs after reflow: at 170 °C for 10 min **a** solder/Cu substrate, **b** solder/Cu particle, and at 200 °C for 50 min **c** solder/Cu substrate, **d** solder Cu/particle

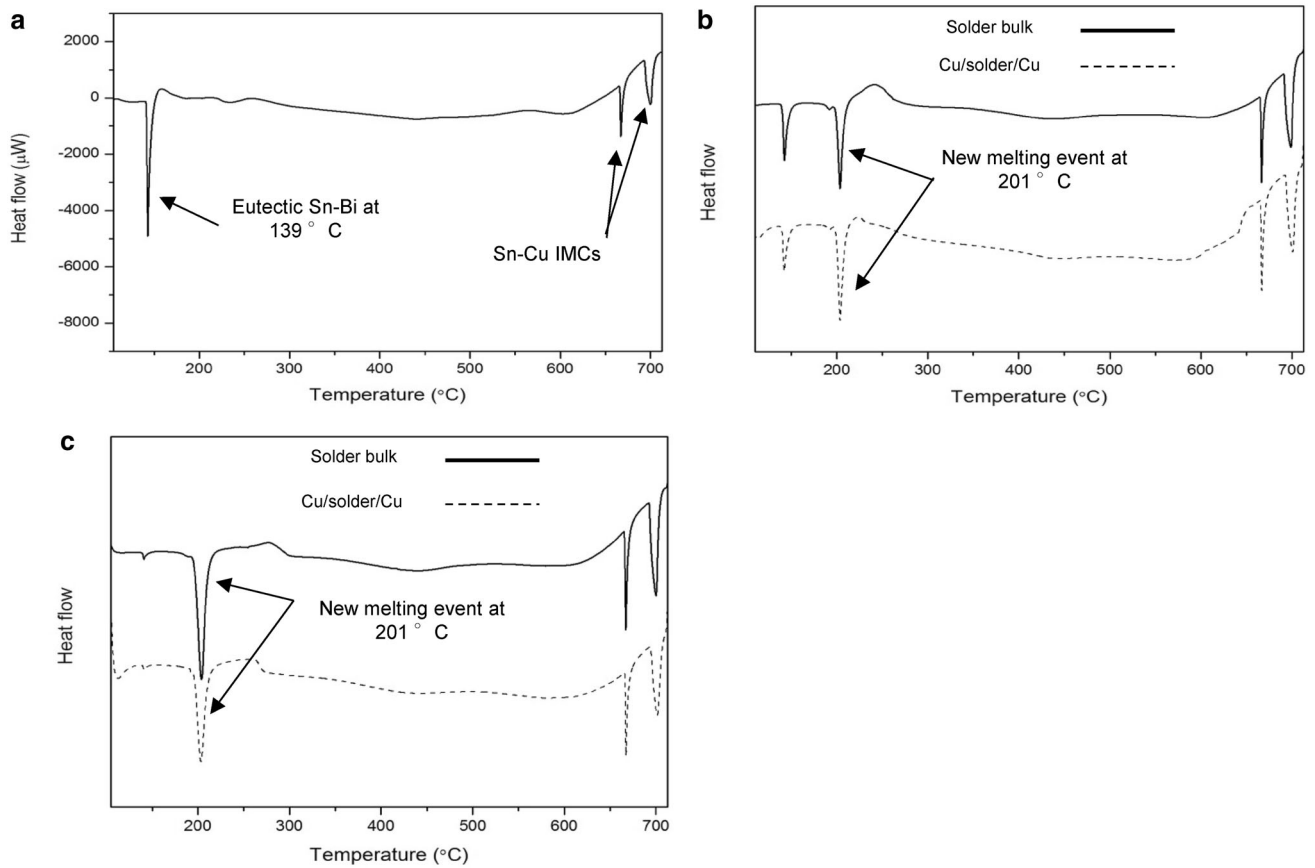


Fig. 10 The DSC results of Sn–Bi–30Cu **a** before reflow (paste), **b** after reflow at 200 °C for 10 min, and **c** after reflow at 200° for 50 min

By integrating the area of the endothermic melting valleys, the specific heat of fusion, Δh_f , for each reflow profile can be determined [17]. Therefore, the remaining eutectic phase can be quantified with Eq. (2):

$$\text{Remaining eutectic phase (\%)} = \left(\frac{\Delta h_{f_Avg}}{\Delta h_{Eutectic}} \right) \times 100 \quad (2)$$

where Δh_{f_Avg} is the average of two samples per reflow profile. The results are summarized in Tables 2 and 3, and

Table 2 Results of DSC experiments with Sn–Bi solder with added Cu particle

Reflow temperature (°C)	Reflow period (min)	Solder bulk				
		1st peak			2nd peak	
		Melting onset (°C)	Melting range (°C)	Remaining eutectic phase (%)	Melting onset (°C)	Melting range (°C)
170	1	138.8	4.0	80.3	201.0	2.2
	10	139.1	3.8	55.2	201.1	3.8
	50	138.2	3.2	13.7	201.0	4.7
200	1	139.1	3.4	66.5	200.5	2.2
	10	138.1	2.7	37.9	197.4	6.3
	50	137.0	3.1	3.3	194.8	10.4
230	1	138.8	3.0	28.1	199.2	5.3
	10	137.7	2.9	11.4	194.9	10.4
	50	137.5	3.5	4.1	192.8	12.7

Table 3 Results of DSC experiments with Sn–Bi solder with added Cu particle between Cu substrates

Reflow temperature (°C)	Reflow period (min)	Cu/solder/Cu				
		1st peak			2nd peak	
		Melting onset (°C)	Melting range (°C)	Remaining eutectic phase (%)	Melting onset (°C)	Melting range (°C)
170	1	138.7	2.5	97.0	200.3	2.9
	10	138.6	2.6	79.0	200.4	3.3
	50	138.2	2.7	22.3	200.4	4.8
200	1	138.2	3.0	66.7	199.6	3.3
	10	138.1	2.3	30.2	198.4	5.3
	50	137.5	2.4	3.2	194.1	10.7
230	1	137.7	3.0	27.8	198.3	5.5
	10	137.9	2.4	7.2	194.1	10.6
	50	137.2	2.8	2.9	192.3	12.3

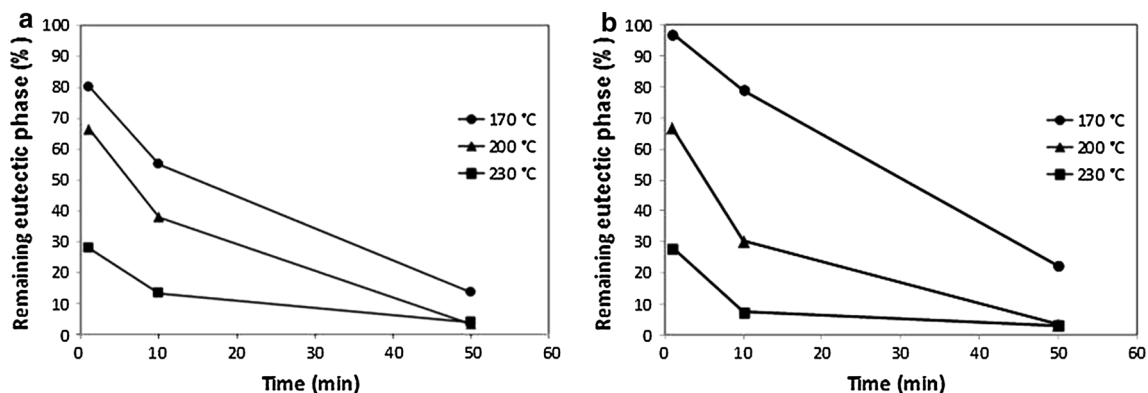
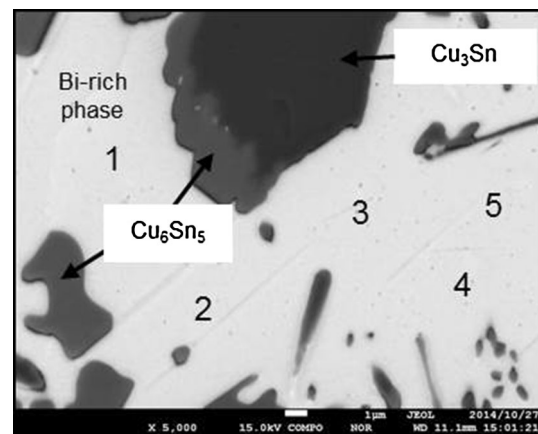
**Fig. 11** Remaining eutectic phase for each reflow profile: **a** solder bulk with Cu particle additions and **b** solder with Cu particle additions between Cu substrates

Fig. 11. As can be seen, increasing the reflow period or temperature increases the percentage of the Sn phase that reacts with the Cu. Furthermore, even though the percentage of the remaining eutectic phase is slightly lower for the bulk solder sandwiched between Cu substrates when subjected to higher heat inputs, it appears that the effect of Cu atoms from the substrates on consuming the Sn phase is negligible when compared to that of the added Cu particles.

4.5 The investigation on the new melting event

To investigate the newly appeared melting event, the elemental composition was determined via EPMA, with the results shown in Fig. 12 and Table 4. As can be seen, Sn and Cu are present in the Bi-rich phase. To investigate the phases present in the sample in more detail, XRD analysis was also performed. Figure 13 shows the X-ray diffraction pattern of the solder after being reflowed at 200 °C for 50 min. By matching the results with data from the International Centre for Diffraction Data, it appears that all the peaks are identified

**Fig. 12** Back-Scattered image of the solder after reflow at 200 °C for 50 min. Numbers (1–5) represent the atomic composition analysis spots performed by EPMA which illustrated at Table 4

exhibiting Bi phase with the highest intensity which co-exists with Sn, Cu, Cu_6Sn_5 , and Cu_3Sn phases. In addition, there is no sign indicating formation of a new phase.

Table 4 The quantitative results of atomic composition analysis by EPMA

	Atomic (%)				
	1	2	3	4	5
Cu	4.54	5.73	5.92	3.99	5.61
Sn	1.79	1.74	1.68	1.29	5.71
Bi	93.67	92.53	92.40	94.72	88.67

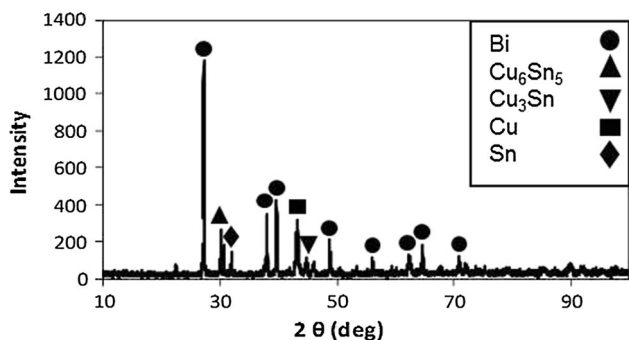


Fig. 13 XRD pattern of the Sn–Bi–30Cu solder after reflow at 200 °C for 50 min

4.6 Theoretical investigation on Cu particles size-effect and their enhanced free energy

In addition to the pronounced advantages of particle addition in TLP bonding process, application of particles can provide a further advantage. Based on the analysis by Porter and Easterling [31], if a solvent phase, α , is acted on by a pressure of 1 atm, a very small solid particle, β , in the α phase is subjected to an extra pressure ΔP , because of the curvature of the α/β interface. ΔP can be quantified with Eq. (3) [31]:

$$\Delta P = \frac{2\gamma}{r} \tag{3}$$

where γ , is the α/β interfacial energy and r is the radius of the spherical particle. According to the “PV” term in the Gibbs free energy, an increase in P increases the free energy, G, when the system is kept at a constant temperature, as shown in Eq. (4) [31]:

$$\Delta G = \Delta P \cdot V \tag{4}$$

Therefore, by combining Eqs. (3) and (4), the free energy increases as the curvature of the α/β interface increases, which can be calculated with Eq. (5) [31, 32]:

$$\Delta G_\gamma = \frac{2\gamma V_m}{r} \tag{5}$$

where V_m is the molar volume of the β phase. This increase in G due to the interfacial energy is known as the capillary

effect or Gibbs–Thomson effect. By assuming the α phase is a regular solution and the β phase is a nearly pure phase, Eq. (6) is obtained [31]:

$$C_r = C_\infty \exp \frac{2\gamma V_m}{RT r} \tag{6}$$

where C_r is the equilibrium concentration of the solute across a curved interface, C_∞ is the equilibrium concentration of the solute across a planar interface, R is the gas constant, and T is the absolute temperature. For small values of the exponent, Eq. (6) can be simplified into Eq. (7):

$$C_r \cong C_\infty \left(1 + \frac{2\gamma V_m}{RT r} \right) \tag{7}$$

Using $\gamma = 2500 \text{ mJ/m}^2$ (assumed to be the incoherent solid/solid interfacial energy) [33, 34], $V_m = 7.11 \times 10^{-6} \text{ m}^3/\text{mol}$, $R = 8.31 \text{ J/mol K}$, and $T = 500 \text{ K}$ gives Eq. (8):

$$\frac{C_r}{C_\infty} \cong 1 + \frac{2.73 \times 10^{-9}}{r} \tag{8}$$

Finally by using $r = 2.5 \mu\text{m}$ in Eq. (8), $C_r/C_\infty \approx 1.003$. This ratio appears to be negligible for particles in the range of micron-size; however, in addition C_r/C_∞ ratios for the case of small particles with a higher curvature (smaller diameters) were investigated theoretically. The C_r/C_∞ ratios for the Cu particles with the diameter of 500 and 100 nm were estimated to be 1.03 and 1.17, respectively. These results show that particles in the range of nano-size would have an additional effect in accelerated consumption of the Sn phase.

5 Discussion

In this section, the isothermal solidification of Sn–Bi solder joint will be discussed. This will be followed by a discussion of the changes in composition due to the TLP bonding process.

5.1 Isothermal solidification of Sn–Bi solder joints

The microstructure analysis of the Sn–Bi solders with and without added Cu particles after being subjected to high heat inputs were conducted and the former revealed the formation of extensive networks of Sn–Cu IMCs, which is consistent with the results reported by other researchers [22]. In addition, the isothermal solidification as a result of consumption of the entire Sn phase in Sn–Bi solder joints with and without added Cu particle was investigated using SEM. Complete isothermal solidification was achieved in Sn–Bi solder joint with added Cu particles after reflow at 200 °C for 50 min

while Sn–Bi solder joint without added Cu particles did not achieve complete isothermal solidification even after reflow at 230 °C for 6 h indicating the advantage of using particles in accelerating the isothermal solidification.

5.2 The spalling of Cu_6Sn_5

The spalling of the Cu_6Sn_5 IMC in this research occurred through two driving forces: the compressive stress during the early stages of reflow and the thermodynamic force during the final stages of reflow. As can be seen in Fig. 9b, after being reflowed at 170 °C for 10 min, the Cu_6Sn_5 IMCs have spalled away from the Cu particle, while the Cu_6Sn_5 IMCs remain attached to the Cu substrate. As was reported by other researchers, as the IMC layer becomes thicker it generates a compressive stress, σ , which eventually results in the spallation of the IMCs [35]. Here, the driving force for spalling during the early stages of reflow can be attributed to a similar phenomenon where, because of the curvature of the Cu particles, the compressive stress is split into two forces, one pointing towards the neighboring grain and the other in-line with the center of the Cu particle, but pointing outwards. Accordingly, the latter provides the driving force that causes the IMCs to spall away from the Cu particles, as shown in Fig. 14b. However, the magnitude of the driving force required for the IMCs on a Cu substrate to spall away is higher (Fig. 14a).

The second type of spalling that occurs during the final stages of reflow appears to be a typical example of massive spalling. Massive spalling occurs once the original reaction product at the interface is no longer in local thermodynamic equilibrium with the solder, resulting in the massive spalling of interfacial IMCs away from the original location to provide room for the nucleation and growth of the equilibrium phase [36, 37]. One common case of massive spalling that has been previously reported is the spalling of Cu_6Sn_5 during the reaction between Sn–3Ag–0.5Cu on Au/Ni substrates. In this case, the initial concentration of Cu in the solder is low, and because of the reactions that occur, the concentration of Cu decreases significantly as the concentration of the Cu_6Sn_5 phase increases, which results in the spalling of Cu_6Sn_5 [36]. However, in some cases, the decreasing Sn concentration as the formation of Cu_6Sn_5 increases can also induce massive spalling [36, 38]; this phenomenon has occurred in the present study. The added Cu particles react with a large amount of Sn in the solder joint, and thus, there is a sudden drop in the concentration of Sn in the solder joint while there is no concentration drop of Cu as is not entirely consumed. This new driving force results in the massive spalling of Cu_6Sn_5 from both the Cu particles and substrates into the solder to achieve local thermodynamic equilibrium. As can be seen in

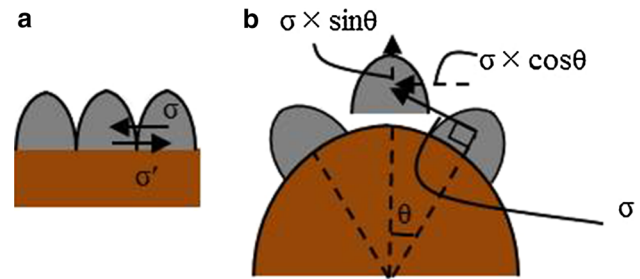


Fig. 14 Illustration of compressive stresses between Sn–Cu IMCs on a **a** Cu substrate and **b** Cu particle

Fig. 9c, d, after being reflowed at 200 °C for 50 min, the spalling of Cu_6Sn_5 has occurred at both the Cu particles and substrates.

5.3 The effect of the large surface area of the Cu particles on the DSC results

As was mentioned in Sect. 1, the larger ratio of surface area to volume of the particles compared to planar substrates is another advantage of using particles in the TLP bonding process. Therefore, the contribution of Cu flux from the particles and substrates as a function of the surface area:volume ratio has been investigated. It is well established that the dissolution of a solid metal in a liquid metal can be quantified with Eq. (9) [39, 40]:

$$\frac{dc}{dt} = k \frac{S}{v} (c_s - c) \quad (9)$$

where c is the concentration of the dissolved metal in the liquid metal (kg m^{-3}), t is the time (s), c_s is the saturation concentration (kg m^{-3}), k is the dissolution rate constant (m s^{-1}), S is the surface area of the solid specimen (m^2), and v is the volume of the melt (m^3). Therefore, the flux of Cu atoms into the melt is proportional to the ratio of the surface areas (S) of the Cu sources (particles and substrates). Thus, the surface area of the Cu particles and substrates were determined. The mean weight of a solder joint before reflow was on average 0.0269 g (5 measurements, standard deviation = 9.28×10^{-4}) with a volume of 3.93 mm^3 . By assuming all the Cu particles have a diameter of 5 μm , the total surface area of the Cu particles inside the solder melt is $1.08 \times 10^9 \mu\text{m}^2$, while the Cu substrate above and below the solder have surface areas of 7.07×10^6 and $2.67 \times 10^7 \mu\text{m}^2$, respectively. Therefore, the total surface area of the Cu particles is approximately 40-times larger than the total surface areas of the Cu substrates on both side of the solder. Using similar calculations, the total surface areas of Cu particles and substrates as a function of the particle diameter was estimated, and shown in Fig. 15.

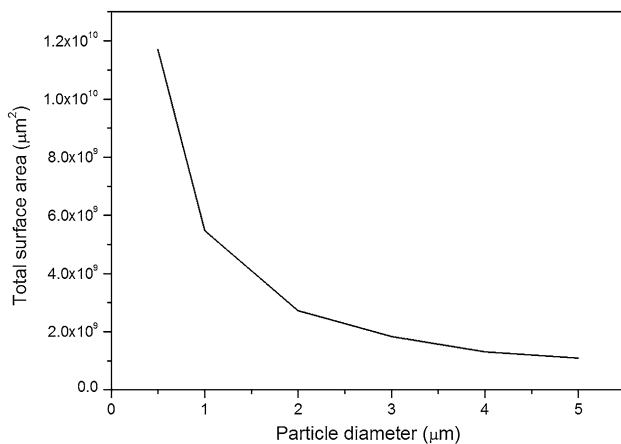


Fig. 15 Estimation of total surface areas of Cu particles and Cu substrate as a function of the particle diameter

The DSC results of the Sn–Bi–30Cu solder before and after reflow at 200 °C for 10 and 50 min were shown in Figs. 10 and 11, and the TLP bonding process with and without Cu flux from the Cu substrates was examined. According to the DSC results, the Cu flux from the substrates proved negligible compared to that of the Cu particles. The insignificant effect of the Cu substrates on the TLP bonding process can be attributed to the trivial surface area of the Cu substrates compared to the large surface area of the Cu particles.

5.4 Analysis of the Bi-rich phase

The presence of Sn and Cu in Bi-rich phase obtained by EPMA elemental analysis and known peaks acquired by XRD, which suggested that the new melting event at 201 °C cannot represent any new phase. By combining these results and considering the Cu–Sn–Bi ternary phase diagram [41], it may suggest that the new melting event represents a mixed phase consists of Bi phase and Sn–Cu IMCs which is consistent with the results reported by D’Hondt and Corbin [22].

6 Conclusions

The microstructures of the Sn–58Bi eutectic solders with and without 30 mass% of added Cu particles were compared after various reflow profiles and the effects of adding Cu particles on the TLP processing of Sn–Bi solder were investigated. The results obtained in this study are summarized below:

1. By adding 30 mass% of Cu particles and being reflowed at 200 °C for 50 min, the Sn phase was successfully consumed by the Cu, leaving Sn–Cu IMCs and a Bi-rich phase in the solder joint.

2. The difference between the equilibrium concentration of the atoms from the added particles with relatively small diameters and the planar substrate was determined, theoretically. Accordingly, the advantages of using fine particles with high curvatures in TLP processing were understood.
3. By adding 30 mass% of Cu particles, the formation of Cu₆Sn₅ results in a sharp decrease in the Sn concentration, which in turn induces massive spalling in the Cu₆Sn₅ layers of both the Cu particles and substrates. The spalling direction is towards the solder to revive the local thermodynamic equilibrium. The spalling of the Cu₆Sn₅ IMCs around the Cu particles occurs earlier in the TLP bonding process compared to that of the Cu₆Sn₅ on the Cu substrates because of the compression stress generated.
4. The new melting event that appeared in the DSC curves at 201 °C is believed to be attributed to the local compositions of Sn–Cu IMCs and Bi in the ternary Cu–Sn–Bi system. Therefore, it could be concluded that the melting point of the Sn–Bi solder was increased by approximately 62 °C.
5. The DSC results of the solders formed with and without Cu substrates were compared, with the results showing the significance of the larger surface area of the Cu particles compared to that of the planar Cu substrates. In addition, the surface area of the Cu particles was found to be approximately 40-times larger than the total surface area of the Cu substrates on both sides of the solder.
6. To achieve the complete conversion of the Sn phase to Sn–Cu IMC phases with lower heat inputs, decreasing the size of the Cu particles is recommended. However, surface modification (e.g., protective coatings) of the Cu particles will be required to prevent oxidation.

References

1. J. Wang, H.S. Liu, L.B. Liu, Z.P. Jin, *J. Electron. Mater.* **35**, 1842 (2006)
2. S.D. Rani, G.S. Murthy, *J. Mater. Eng. Perform.* **22**, 2359 (2013)
3. N.M. Poon, C.M. Lawrence Wu, J.K.L. Lai, Y.C. Chan, *IEEE Trans. Adv. Packag.* **23**, 708 (2000)
4. D.C.C. Lam, J. Wang, F. Yang, *IEEE Trans. Adv. Packag.* **30**, 636 (2007)
5. Y.E. Huang, D. Hagen, G. Dody, T. Burnette, in *IEEE/CPMT Int. El. Mfg.* (Austin, TX, 1998), pp. 105–111
6. T.H. Wang, C.-I. Tsai, C.-C. Lee, Y.-S. Lai, *Microelectron. Reliab.* **53**, 297 (2013)
7. T. Nozu, M. Koshi, H. Yamamoto, J. Masuda, T. Nishimura, *J. Jpn. Inst. Met.* **74**, 485 (2010)
8. S. Zhao, X. Pang, *Microelectron. Reliab.* **49**, 350 (2009)

9. H.R. Kotadia, P.D. Howes, S.H. Mannan, *Microelectron. Reliab.* **54**, 1253 (2014)
10. W.D. Macdonald, T.W. Eagar, *Annu. Rev. Mater. Sci.* **22**, 23 (1992)
11. G.O. Cook III, C.D. Sorensen, *J. Mater. Sci.* **46**, 5305 (2011)
12. M.S. Park, S.L. Gibbons, R. Arroyave, *Acta Mater.* **60**, 6278 (2012)
13. J.F. Li, P.A. Agyakwa, C.M. Johnson, *Acta Mater.* **58**, 3429 (2010)
14. C.C. Lee, Y.C. Chen, *Thin Solid Films* **286**, 213 (1996)
15. J.F. Li, P.A. Agyakwa, C.M. Johnson, *Acta Mater.* **59**, 1198 (2011)
16. R.W. Chuang, C.C. Lee, *IEEE Trans. Compon. Packag. Technol.* **25**, 453 (2002)
17. R.I. Rodriguez, D. Ibitayo, P.O. Quintero, *IEEE Trans. Compon. Packag. Manuf. Technol.* **3**, 549 (2013)
18. C.C. Lee, W.W. So, *Thin Solid Films* **366**, 196 (2000)
19. S.A. Moeini, H. Greve, F.P. McCluskey, Strength and reliability of high temperature transient liquid phase sintered joints, in *International Conference and Exhibition on High Temperature electronics (HiTEC)* (Albuquerque, New Mexico, USA, 2014)
20. H. Greve, S.A. Moeini, F.P. McCluskey, Reliability of paste based transient liquid phase sintered interconnects, in *Electronic Components and Technology Conference (ECTC)* (Lake Buena Vista, Florida, USA, 2014)
21. C.W. Sinclair, *J. Ph. Equilib.* **20**, 361 (1999)
22. T. D'Hondt, S.F. Corbin, *Metall. Mater. Trans. A* **37A**, 217 (2006)
23. J.G. Lee, F. Guo, K.N. Subramanian, J.P. Lucas, *Solder. Surf. Mt. Technol.* **14**, 11 (2002)
24. F. Guo, S. Choi, J.P. Lucas, K.N. Subramanian, *Solder. Surf. Mt. Technol.* **13**, 7 (2001)
25. J.L. Marshall, J. Calderon, *Solder. Surf. Mt. Technol.* **9**, 22 (1997)
26. S. Chada, W. Laub, R.A. Fournelle, D. Shangguan, *J. Electron. Mater.* **28**, 1194 (1999)
27. H.R. Kotadia, A. Panneerselvam, M.A. Green, S.H. Mannan, Limitations of nanoparticle enhanced solder pastes for electronics assembly, in *12th IEEE International Conference on Nanotechnology (IEEE-NANO)* (Birmingham, United Kingdom, 2012)
28. Y. Zhou, W.F. Gale, T.H. North, *Int. Mater. Rev.* **40**, 181 (1995)
29. M.L. Kuntz, Y. Zhou, S.F. Corbin, *Metall. Mater. Trans. A* **37A**, 2493 (2006)
30. Q. Zhang, H. Zou, Z.-F. Zhang, *J. Mater. Res.* **25**, 303 (2010)
31. D.A. Porter, K.E. Easterling, *Phase Transformations in Metals and Alloys*, 2nd edn. (Nelson Thornes Ltd, Cheltenham, 2001), pp. 44–47
32. H.K. Kim, K.N. Tu, *Phys. Rev. B* **53**, 16027 (1996)
33. W.K. Choi, H.M. Lee, *J. Electron. Mater.* **29**, 1207 (2000)
34. J.M. Howe, *Interfaces in Materials* (Wiley, New York, 1997), p. 378
35. M. He, W.H. Lau, G. Qi, Z. Chen, *Thin Solid Films* **462**, 376 (2004)
36. S.C. Yang, C.E. Ho, C.W. Chang, C.R. Kao, *J. Appl. Phys.* **101**, 84911 (2007)
37. H.R. Kotadia, A. Panneerselvam, O. Mokhtari, M.A. Green, S.H. Mannan, *J. Appl. Phys.* **111**, 74902 (2012)
38. K.Z. Wang, C.M. Chen, *J. Electron. Mater.* **34**, 1543 (2005)
39. V.I. Dybkov, *Growth Kinetics of Chemical Compound Layers* (Cambridge International Science Publishing, Cambridge, 1998)
40. V.I. Dybkov, *J. Mater. Sci.* **25**, 3615 (1990)
41. B.J. Lee, N.M. Hwang, H.M. Lee, *Acta Mater.* **45**, 1867 (1997)